From single-cycle self-compressed filaments to isolated attosecond pulses in noble gases

Arnaud Couairon*
Centre de Physique Théorique, École Polytechnique, CNRS, F-91128, Palaiseau, France

Himadri S. Chakraborty
Department of Chemistry and Physics, Northwest Missouri State University, Maryville, Missouri 64468, USA
and Department of Physics and Astronomy, Louisiana State University, Baton Rouge, Louisiana 70803-4001, USA

Mette B. Gaarde
Department of Physics and Astronomy, Louisiana State University, Baton Rouge, Lousiana 70803-4001, USA
(Received 20 December 2007; published 15 May 2008)

We investigate numerically the recently proposed technique of pulse self-compression by filamentation in noble gases. We show that propagation of a 30 fs infrared pulse containing a few mJ of energy leads to a few-cycle pulse in xenon, krypton, argon, and neon. We describe the different mechanisms and stages of self-compression in the different gases and show that neon, with the highest ionization potential, allows compression to the shortest durations and highest peak intensities. We discuss the process by which an unavoidable frequency modulation of the self-compressed filament simultaneously allows the generation of isolated attosecond (as) pulses via high-order harmonic generation and limits the conversion efficiency of the as pulses.

DOI: 10.1103/PhysRevA.77.053814 PACS number(s): 42.65.Re, 42.65.Ky, 42.65.Jx, 32.80.Wr

I. INTRODUCTION

Many physical processes of interest such as the electronic and atomic rearrangements in chemical reactions, and the structural changes in optical media interacting with intense laser pulses occur at subfemtosecond time scales [1,2]. Measurements with attosecond (1 as$=10^{-18}$ s) time resolution of these processes are so far based on the use of coherent extreme ultraviolet pulses of a few hundreds of as generated by upconversion of near infrared frequencies from conventional ultrashort laser pulses via high-order harmonic generation (HHG) in a gas jet. In order to produce routinely available, intense, well controlled, few-cycle infrared laser pulses from which subfemtosecond pulses can be obtained, several compression schemes have been already proposed. Among these schemes, the gas-filled hollow fiber technique takes advantage of the guiding property of the fiber which maintains a high intensity over a long path, thus inducing spectral broadening due to self-phase-modulation [3]. Subsequent recompression in a broadband dispersive system allows for the generation of 5 fs sub-mJ pulses.

A recently proposed alternative technique that potentially leads to few-cycle pulses at higher energies is based on the nonlinear effects occurring in femtosecond filamentation [4,5]. Filamentation in argon from a 1 mJ, 30 fs infrared laser pulse was recently shown to generate a nearly single-cycle pulse by itself [6–8]. Experiments have shown that two-cycle pulses were obtained after a double filamentation process followed by recompression via chirped mirrors at the end of each cell so as to compensate the dispersion induced by the exit windows. The measured spectra indicate, however, that Fourier transform limited pulses could be achieved by suitable chirp compensation. For a broad range of parameters of the input pulse (with durations smaller than 50 fs), simulations modeling filamentation in a constant pressure gas cell predict the generation of a single-cycle pulse at the end of the filament [6,7]. Due to spatiotemporal conical emissions from the filament core which occur generically for filaments in all types of media [9,47], the shortest duration of a self-compressed filament actually depends on the spatial selection of the on-axis part of the filament [10]. In practice, the duration of this structure increases when it propagates through any normally dispersive optical element thus justifying the use of chirped mirrors to recover the few-cycle pulses in experiments. To avoid dispersion as well as the extraction stage, it was proposed and shown from numerical simulations that a bell-shaped gas pressure gradient enables a control of the nonlinearities acting in the filamentation process [11]. In this case, a single-cycle pulse is obtained and propagates without any change in duration beyond the pressure gradient.

Single-cycle pulses produced by filamentation exhibit a characteristic feature which influences the generation of high-order harmonics and attosecond pulses [12]: We showed that the duration of harmonic radiation generated by the few-cycle structure extracted from a self-compressed filament is limited not only by the rapid variation of the driving pulse intensity, but also by its chirp. This chirp constitutes a frequency gate for the generation of the highest-order harmonics in the sense that the cutoff frequency is lowered by the sharp increase of the instantaneous frequency of the driving pulse. Recombination of a selected range of high-order harmonics immediately beyond the cutoff was shown to produce isolated attosecond pulses [12].

In the present paper, we investigate the generation of single-cycle pulses by filamentation in different noble gases, and we discuss the conditions for the generation of isolated attosecond pulses. The different noble gases lead to different

*couairon@cpht.polytechnique.fr

saturation intensities within the filament, interpreted in terms of a competition between the optical Kerr effect and the defocusing effect induced by the plasma generated by optical field ionization. These intensities, as well as the time-frequency gate formed by the self-compressed filament, determine the structure of the spectrum of high-order harmonics generated by interaction of the driving pulse with a low-pressure gas, and therefore of the final attosecond pulses.

The outline of the paper is the following: In Sec. II we discuss our theoretical models for filamentation-driven self-compression and for high-order harmonic generation. In Sec. III we present our results for self-compression in different noble gases, and show that it is possible to obtain few-cycle pulses in xenon, krypton, argon, and neon. We investigate the influence of the gas density and ionization potential on the properties of the self-compressed pulse, and show that the lighter noble gases with higher ionization potentials allow for the generation of shorter and more intense pulses. In Sec. IV we present results of high-order harmonic generation by few-cycle pulses generated via self-compression in neon. We discuss the influence of the time-dependent frequency and the absolute phase of the driving pulse on the time structure of the generated harmonics. Finally, in Sec. V we summarize our results.

II. MODEL

A. Filamentation model

The numerical code used for the simulations of filamentation relies on the physical model developed for the nonlinear propagation of an intense laser pulse in Kerr media [4] which was shown to successfully reproduce various types of experimental situations in gases [13,14], or in condensed media [15–19].

The laser pulse evolution along the propagation axis z is simulated by solving Eqs. (47)–(51) in Ref. [4] which are valid under the slowly evolving wave approximation to describe the propagation of pulses as short as one optical cycle. The model includes the effects of diffraction, group velocity dispersion, the optical Kerr effect (with nonlinear refraction index coefficient n_2), self-steepening and space-time focusing, plasma generation, plasma defocusing, and nonlinear losses corresponding to the energy necessary for ionization (see Ref. [20] for details).

B. Physical parameters

The 800 nm input pulse duration is $\tau_{\mathrm{FWHM}}=30$ fs (full width at half-maximum, FWHM). The beam is sufficiently narrow ($w_0 \sim 500$ μm) so as to avoid a too large self-focusing distance before filamentation. The physical parameters of noble gases used in our model are summarized in Table I and were obtained as indicated below.

Nonlinear refractive index. We use the values of the nonlinear refractive index n_2 deduced from the measurements of the hyperpolarizability $\langle\gamma\rangle$ by Shelton [21]. According to Eq. (2) in Ref. [21],

TABLE I. Parameters γ_0, A, and B for the calculation of the hyperpolarizability $\langle\gamma\rangle$ of noble gases by means of Eq. (1), corresponding values of the nonlinear index coefficient n_2, critical power for self-focusing P_{cr}, dispersive coefficients k_0'' and k_0''', ionization potentials U_i, number of photons K, and cross sections involved in multiphoton ionization (σ_K) computed at 800 nm.

	Ne	Ar	Kr	Xe
γ_0 (10^{-63} cm^4/V^3)	7.435	72.75	162.1	429.5
A (10^{-10} cm^2)	−1.924	1.066	1.389	1.499
B (10^{-20} cm^4)	6.901	2.033	3.465	8.048
Computed at 800 nm	Ne	Ar	Kr	Xe
$\langle\gamma\rangle$ (10^{-63} cm^4/V^3)	6.5449	81.3204	188.1451	520.2386
n_2 (10^{-19} cm^2/W)	0.14	1.74	4.03	11.15
P_{cr} (GW)	68	5.5	2.4	0.9
k_0'' (fs^2/cm)	0.0202	0.1980	0.3996	0.9113
k_0''' (fs^3/cm)	0.0158	0.1586	0.3298	0.7836
U_i (eV)	21.564	15.759	13.999	12.130
K	14	11	10	8
σ_K (s^{-1} cm^{2K} W^{-K})	1.7 $\times 10^{-185}$	6.0 $\times 10^{-140}$	5.3 $\times 10^{-125}$	3.0 $\times 10^{-96}$

$$\langle\gamma\rangle = \gamma_0[1 + A\nu_L^2 + B\nu_L^4], \tag{1}$$

where $\nu_L^2=6\nu^2$ and $\nu=\lambda_0^{-1}$ is expressed in cm^{-1}. From Table IV in Ref. [21], we obtain the parameters necessary to calculate n_2 for the noble gases as indicated in Table I.

From the hyperpolarizability, we obtain the third-order susceptibility and the coefficient for the nonlinear refractive index by means of the formulas

$$\chi^{(3)} \simeq \langle\gamma\rangle\rho_{at}/4\epsilon_0, \quad n_2 = \frac{3}{4}\frac{\chi^{(3)}}{n_0^2\epsilon_0 c}. \tag{2}$$

From the nonlinear index, we determine the critical power for self-focusing defined by $P_{\mathrm{cr}} \equiv 3.72\lambda_0^2/8\pi n_0 n_2$ (see Table I), above which the pulse will undergo a catastrophic collapse over a finite distance marking the beginning of filamentation.

Dispersion. Our code describes dispersion by means of frequency-dependent linear refractive index $n(\omega)$ for noble gases, given by Dalgarno and Kingston [22] (see Table I for corresponding second- and third-order dispersive coefficients at 800 nm).

Ionization rates. We used the general formulation of Keldysh [23] and Perelomov *et al.* (PTT) [24] for the ionization rate $W(I)$ with a suitable prefactor determined by Ilkov *et al.* [25], thus covering the regime $I \sim 10^{13}$–10^{14} W/cm^2 of the infrared femtosecond filamentation. Ionization rates around 800 nm calculated within this generalized Keldysh-PPT (KPPT) approach are in good agreement with rates calculated by direct numerical integration of the time-dependent Schrödinger equation within the single active electron approximation. For comparison, self-compression in filaments was also investigated by using multiphoton ionization (MPI)

rates $W_{\mathrm{MPI}}(I)=\sigma_K I^K$ asymptotic to the KPPT ionization rates $W(I)$ at low intensities (cross sections given in Table I).

C. Model for high-order harmonic generation

We extract the laser pulse after it has undergone filamentation-driven self-compression in the long noble gas medium, and use it to generate high-order harmonics in a separate, short, argon gas jet at much lower pressure. The propagation equations for the electric field $\tilde{E}(\omega,r,z)$ of the laser light as well as for the generated xuv light have the following form, in a coordinate system that moves with the laser pulse:

$$\nabla_{\perp}^2 \tilde{E}(\omega)+\frac{2i\omega}{c}\frac{\partial \tilde{E}(\omega)}{\partial z}=\tilde{S}(\omega), \tag{3}$$

under the assumption of the slowly evolving wave approximation [26]. We solve the propagation equations by space marching in the frequency domain, and at each step in the propagation direction use the resulting time-dependent electric field to evaluate the nonlinear source terms in the time domain.

The source term for the laser field is due to plasma defocusing and dispersion. We use KPPT ionization rates to calculate the time-dependent electron density [25]. As the input electric field we use the electric field extracted from the filamentation calculation, choosing an arbitrary carrier-envelope phase (see Sec. IV B below for more details). Due to the short length and low pressure of the argon gas (1 mm and 0.2 atm) the driving field is left almost unchanged during propagation.

The source term for the xuv radiation is the nonlinear polarization field generated by the laser electric field. It is proportional to the density of neutral atoms and the single atom time-dependent dipole moment which is obtained by solving the time-dependent Schrödinger equation using the strong field approximation [27]. We also include reabsorption of the xuv radiation by the argon gas through a frequency-dependent absorption coefficient. More details about our numerical approach to HHG can be found in [28].

III. SIMULATIONS OF FILAMENTATION AND SINGLE-CYCLE PULSE GENERATION

Pioneering numerical simulations of femtosecond filamentation in argon were performed by Mlejnek *et al.* [29] who showed that plasma effects prevail over dispersive effects in the regime of low pressures ($p<10$ atm). In this case, ultrashort laser pulses generate filaments after a self-focusing stage and the evolution of the temporal profile is mainly driven by a competition between multiphoton absorption, plasma defocusing, and Kerr self-focusing. By depleting the intense part of the pulse, multiphoton absorption usually reshapes pulses that underwent a self-focusing stage into double peak temporal profiles while the peak intensities remain around–10^{13}–10^{14} W/cm^2. The formation of these twin subpulses is quite standard in the field of femtosecond filamentation [4]. Starting from a 100 fs pulse easily leads to ~10 fs subpulses [13]. However, the use of these short pulses for applications in attosecond pulse generation is limited if they cannot be isolated. Uneven dispersive terms in low-pressure gases are in general not sufficient to induce an asymmetry and separate these subpulses. However, plasma defocusing occurring in the trail of the pulse which generated the ionization front constitutes an efficient self-action in filaments for shortening and isolating a short subpulse from its twin. This effect was identified as a nonlinear reshaping process by Sergeev *et al.* [30] when only ionization and associated plasma defocusing is considered. In filaments, the scenario identified by Sergeev *et al.* is slightly modified in the sense that the Kerr effect competes with both plasma defocusing and MPA, as shown by Mlejnek *et al.* [31,32], leading generically to refocusing subpulses. This was called spatial replenishment of light [31]. The subpulses initially generated by MPA-induced depletion rapidly desynchronize [14,33], leading to the formation of clean, isolated, self-shortened filaments at a few propagation distances separated by domains where multipeaked structures prevail [7,34]. In contrast with Ref. [32], the main results presented in this paper were obtained with KPPT ionization rates. This leads to higher saturation intensities than those obtained with MPI rates, as shown by the comparison presented in Sec. III D.

A. Filaments in xenon and krypton

Xenon and krypton have ionization potentials close to that of oxygen and should therefore behave similarly to air, regarding ionization. Self-focusing in noble gases, however, is purely instantaneous as it does not include a delayed Raman-Kerr contribution due to rovibrational motion of molecules.

Figure 1 presents numerical simulation results which show typical features of a filament in xenon for a pulse energy of $E_{\mathrm{in}}=2$ mJ and the duration $\tau_{\mathrm{FWHM}}=30$ fs ($P_{\mathrm{in}}=12.8P_{\mathrm{cr}}^{(\mathrm{Xe})}$). The peak intensity in the filament [solid curve in Fig. 1(a)] and the electron density in the wake of the filament [dashed curve in Fig. 1(a)] show that two separated plasma channels are generated successively. Going into finer details, each filament exhibits at least two stages separated by a notch in the electron density (dashed) curve: The first stage corresponds to the self-shortening of the leading part of the pulse and defocusing of the trail. The second stage corresponds to the refocusing of the trailing pulse. Two sets of these two stages are clearly visible on the evolution of the on-axis temporal profile of the intensity displayed in Fig. 1(c); each set is characterized by a V-shaped pattern which features the motion of the leading and trailing pulses that move faster and slower than the group velocity of a pulse with central frequency ω_0, respectively. The slopes of the V branches indicate the velocity of the leading or trailing peaks. Figure 1(b) shows the pulse duration of the radially averaged temporal profiles, the averaging being performed by integration over a diameter of 50 μm larger than that corresponding to the filament. For each pulse, the self-compression process is identified as a decreasing part of the curve in Fig. 1(b). Note that it is discontinuous because of the occurrence of several subpulses during propagation, whereas we follow only that with maximum intensity.

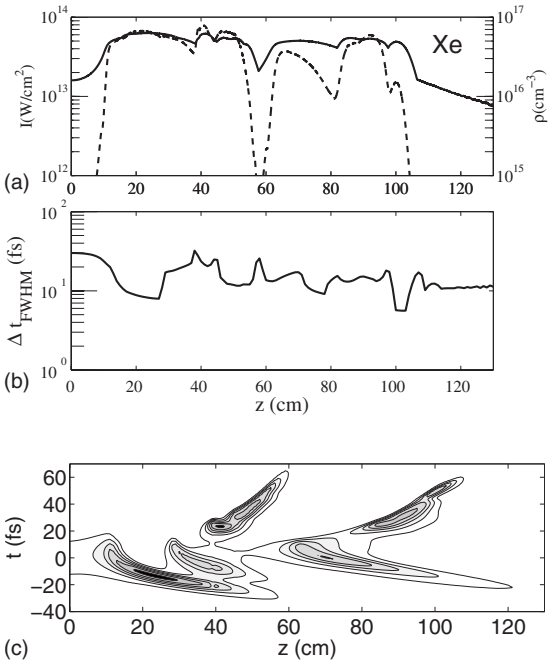

FIG. 1. Simulation of a self-compressed filament in xenon (ionization with KPPT rates). (a) Intensity (solid curve, left-hand axis) and electron density (dashed curve, right-hand axis) vs propagation distance. (b) FWHM duration of the intensity integrated over 50 μm in the radial direction. (c) Evolution of the on-axis temporal profile of the intensity vs propagation distance. The contours indicate intensities from 10^{13} W/cm^2 to 6×10^{13} W/cm^2.

Figure 2 shows results obtained for krypton. In this case, the energy of the input pulse was $E_{\mathrm{in}}=2$ mJ ($P_{\mathrm{in}}=4.6P_{\mathrm{cr}}^{(\mathrm{Kr})}$). The general features are similar as in xenon except that a single plasma channel is obtained. The absence of refocusing of the leading subpulse is due to the smaller power ratio $P_{\mathrm{in}}/P_{\mathrm{cr}}$ in the case of krypton (for the same energy and pulse duration). Notably, the maximum intensity is slightly larger in krypton (9×10^{13} W/cm^2) than in xenon (6×10^{13} W/cm^2) but the maximum electron density is smaller in xenon (4×10^{16} cm^{-3}) than in krypton (8×10^{16} cm^{-3}). In Sec. III B, we compare these saturation values with those obtained in argon and neon.

Figure 2(d) shows the evolution of the space-time intensity distribution within the filament and illustrates well the two possibilities to obtain a self-compressed pulse in the filament: At $z=0.3$ m, the pulse has the shape of a horn after undergoing depletion of its central part due to MPA and plasma induced defocusing of its trailing part. Here the self-shortened pulse consists of the leading time slices. The subsequent evolution of the pulse shows the refocusing process of the trailing part (spatial replenishment scenario [31]). After this stage, a second self-shortened pulse consisting in the trailing time slices is obtained around $z=0.6$ m. The shortness of the refocused pulse depends on several factors: If it becomes sufficiently intense so as to trigger ionization again as is the case at $z=0.55$ m, the plasma density further depletes the trailing part which can shorten the pulse even more until dispersion stops the process. The contrast of this refocused pulse depends on the asymmetry between leading and trailing parts, i.e., the larger the separation between two refocusing events the better is the contrast.

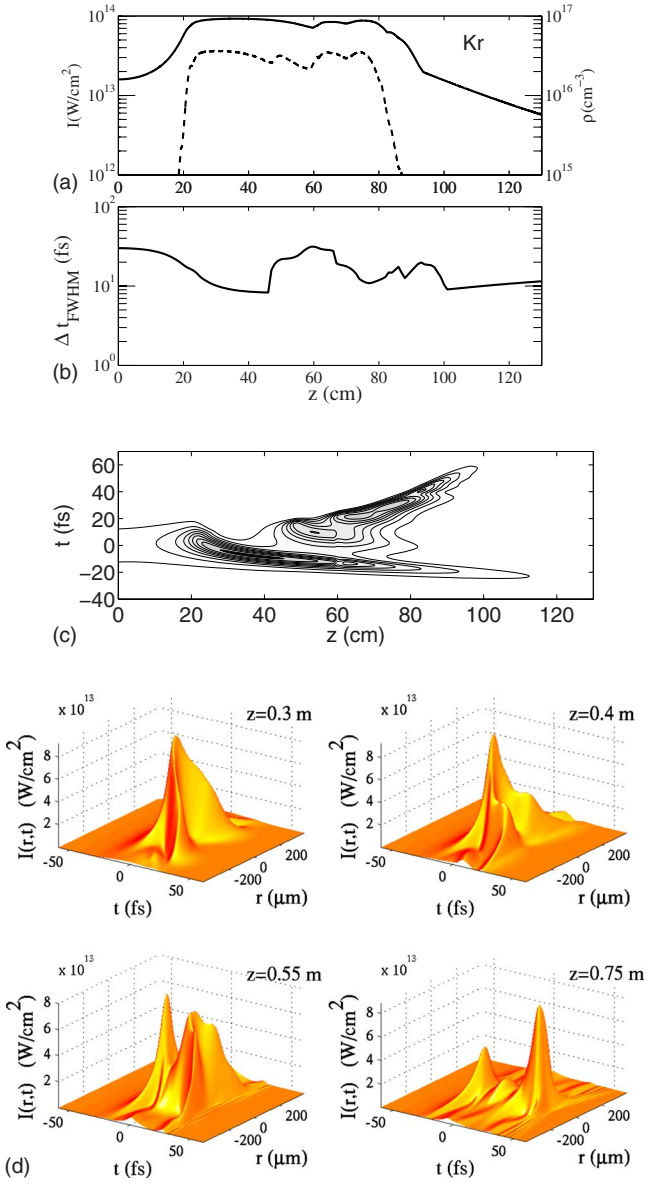

FIG. 2. (Color online) (a)–(c) Same as in 1 but for krypton. The contours in (c) indicate intensities from 10^{13} W/cm^2 to 9×10^{13} W/cm^2. (d) Intensity distribution vs the radial r and time t coordinates at different propagation distances.

B. Argon and neon

Figure 3 shows the peak intensity, the electron density, and the pulse duration during the propagation of a 30 fs infrared laser pulse in argon [Figs. 3(a) and 3(b)] or in neon [Figs. 3(c) and 3(d)]. In particular, the intensities ($>10^{14}$ W/cm^2) reached within the filament are larger than those obtained for krypton and xenon. The pulse durations of the self-compressed pulses are as short as 5–6 fs on a long plateau in argon, and 3–4 fs over a few cm in neon. Simulations of filaments in gases lead as a general standard to compressions down to 8–10 fs [4]. The pulses obtained in

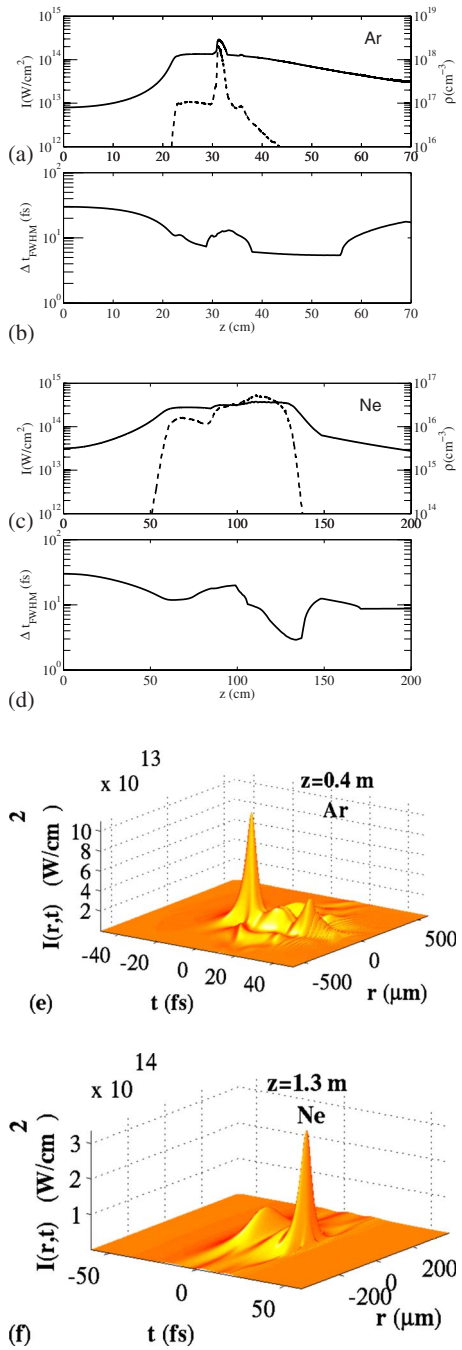

FIG. 3. (Color online) Simulation results for self-compression by filamentation in argon (a,b,e) and neon (c,d,f) at 1 atm. (a,c): Intensity (solid curve, left-hand axis) and electron density (dashed curve, right-hand axis) vs propagation distance. (b,d) FWHM duration of the intensity integrated over a diameter of 40 μm in the radial direction (solid curve, left-hand axis). (e) Intensity distribution of the 7 fs isolated leading peak obtained in argon. (f) Same as in (e) but for neon and 4 fs.

this work constitute the shortest and most intense self-compressed filaments in gases.

The space-time intensity distributions shown in Figs. 3(e) and 3(f) illustrate again the two different possibilities to obtain a self-shortened pulse within the filament: (i) For argon, the short pulse is on the leading part, while the trailing part

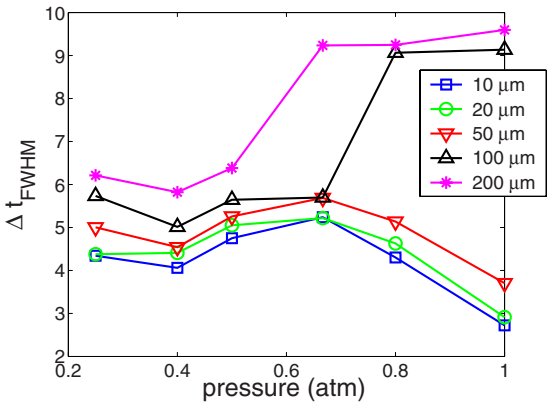

FIG. 4. (Color online) Pulse duration (FWHM) of self-compressed filaments obtained by simulations in neon at pressures from 0.25 to 1 atm. Each curve indicates the durations computed after radially integrating the intensity distribution over a given radius, from 10 to 200 μm.

exhibits a low intensity peak. The latter is the remnant of a refocused pulse that has almost completely depleted by MPA and also defocused by the plasma generated by the leading pulse. (ii) For neon, the isolated self-compressed pulse lies on the trail of the input pulse and it is the leading pulse which was absorbed by MPA and diffracted—a situation similar to what is seen for krypton (Fig. 2).

C. Pressure dependence study of few-cycle filament formation in neon

In neon, we have studied the influence of the pressure on the duration of the few-cycle pulse generated by filamentation. We have kept the product of the input pulse energy and the gas pressure constant so as to perform an investigation at fixed ratio $P_{in}/P_{cr} \simeq 1.7$. For each gas pressure, we have extracted the self-compressed pulse from the filament and computed FWHM duration of the radially averaged intensity distribution, i.e., the duration of the temporal profile of the power contained in cylinders of different radius.

In Fig. 4, we summarize these results and plot the duration of the maximally compressed pulses as a function of gas pressure. Note that the full width at half-maximum (FWHM) duration of the pulse also varies with the radius over which we choose to integrate the intensity distribution. In order to interpret the curves in Fig. 4, note that filament diameters are larger at low pressures [35,36]. At pressures close to 1 atm, the power contained in a cylinder of radius larger than 50 μm encompasses not only the filament core which underwent self-compression, but also a nonfilamented part of the beam and the conical emission—both of longer duration than the filament core. Since the weight of this possible long radiation within the external part of the cylinder is larger than the weight corresponding to the filament core, the overall duration is relatively long (9–10 fs) for large integration radius. For integration radius smaller than the filament radius, the pulse duration corresponds to 3–5 fs, i.e., within one to two optical cycles at 800 nm. There are, therefore, two domains of interest: (i) Around 0.4 atm where the filaments

TABLE II. Comparison of saturation intensities within the filament predicted from model (5) and obtained by full numerical simulations with MPI rates.

Computed at 800 nm	Neon	Argon	Krypton	Xenon
I_{sat}^{pred} (10^{14} W/cm^2)	1.4	0.91	0.77	0.65
I_{sat}^{num} (10^{14} W/cm^2)	0.8	0.6	0.4	0.3

TABLE III. Comparison of saturation intensities within the filament predicted from model (6) and obtained by full numerical simulations with KPPT ionization rates.

Computed at 800 nm	Neon	Argon	Krypton	Xenon
I_{sat}^{pred} (10^{14} W/cm^2)	3	1.1	0.89	0.67
I_{sat}^{num} (10^{14} W/cm^2)	3	1–2	0.9	0.6

have diameters up to 200 μm and remain shorter than 6 fs, and (ii) at 1 atm and above where filaments are narrower ($r \sim 50$ μm) and show shorter duration of 3–4 fs. In terms of energy, the pressure range around 0.4 atm is favored since the self-compressed filaments are larger and slightly longer for a saturation intensity that is not varying with pressure. In Sec. IV below, we use self-compressed pulses from both of these domains to generate high-order harmonics and attosecond pulses.

D. Saturation intensity vs ionization rates

For all the noble gases, we have also investigated the effect of using multiphoton ionization (MPI) rates, $W(I) = \sigma_K I^K$. Although the results are quantitatively different for MPI rates than for KPPT rates, the general scenario for self-compression was found to be robust with respect to this change of ionization rates. In particular, few-cycle self-compressed filament could be obtained with MPI rates as well. The notable differences are the location of the shortest structures for a given gas and the saturation intensity. MPI rates are known to be overestimated with respect to KPPT rates. The saturated intensities obtained in the case of KPPT rates will therefore be higher and are more likely to represent the peak intensities expected in experiments. Thus, we limit the presentation of our simulation results with MPI rates to the discussion of the obtained saturation intensities and their comparison with those obtained with KPPT rates.

Argon and neon have larger ionization potentials than xenon and krypton. Thus, it is more difficult to ionize these gases and the saturation of self-focusing should occur in argon or neon filaments at larger intensities than those reached in xenon or krypton. In order to estimate these intensities at the saturation, we consider the local balance between the refractive index changes due to the Kerr effect and plasma defocusing,

$$n_2 I = \frac{\rho(I)}{2\rho_c}, \tag{4}$$

where a rough estimate of the electron density $\rho(I) \sim W(I)\rho_{at}\tau_p$ allows an expression of the predicted saturation intensity I_{sat}^{pred}. In the limit where the ionization rates are given by the multiphoton regime, $W(I) = \sigma_K I^K$ and

$$I_{sat}^{pred} = \left(\frac{2n_2\rho_c}{\sigma_K \tau_p \rho_{at}} \right)^{1/(K-1)}. \tag{5}$$

An expression of I_{sat}^{pred} which includes the effect of diffraction is given by Eq. (20) in Ref. [4]; the scaling is the same as in (5) but the factor 2 is replaced by 0.76. Table II displays the expected intensities for the different noble gases and the values obtained in our simulations where τ_p was replaced by the duration of the few-cycle self-compressed pulse. As expected, the saturation intensity increases for gases with large ionization potential. The agreement between intensities predicted by (5) and those obtained in full simulations is rather good considering the simplicity of model (5).

In the case of KPPT ionization rates, the complicated expression for $W(I)$ does not allow for an analytical formula. However, we give a numerical solution to

$$n_2 I = \frac{W(I)\rho_{at}\tau_p}{2\rho_c}. \tag{6}$$

In other words, we calculated the predicted saturation intensity I_{sat}^{pred}, for which the line $y = n_2 I$ intersects the curve $y = W(I)\rho_{at}\tau_p/2\rho_c$. Table III displays the saturation intensities predicted from Eq. (6) and the values obtained in our simulations for the different noble gases. Both sets are in good agreement and show that neon leads to the highest peak intensities of the self-compressed filaments.

E. Rapid blueshift of instantaneous frequency

Filaments in neon have the largest saturation intensity and are therefore the most obvious source for few-cycle pulses to be subsequently used for harmonic generation. However, the high saturation intensity also leads to a rapid blueshift of the instantaneous frequency in the self-compressed pulse. This can be understood from standard self-phase modulation theory which predicts an instantaneous frequency shift of

$$\omega(t) \sim \omega_0 - \frac{n_2\omega_0}{c}\int_0^z dz \frac{\partial I(z,t)}{\partial t}. \tag{7}$$

This shows that a larger peak intensity for a similar duration gives a larger trailing slope, and thus a larger blueshift. A high peak intensity also leads to a higher plasma density which gives rise to enhanced self-phase modulation [4]. In addition, self-steepening is more efficient for more intense pulses. Figure 5 shows the on-axis time profiles of the intensity and frequency of the self-compressed filament extracted close to the point of maximum temporal compression for the case of KPPT ionization rates, for the two different pressure ranges of interest, 1.0 atm and 0.4 atm, as discussed in the preceding section. As the intensity of the pulse reaches its peak in time, the instantaneous frequency increases sharply to a value of approximately $2\omega_0$. In the high-pressure case the frequency keeps increasing to almost $4\omega_0$ during the rapid falloff of the intensity, for the low-pressure case the frequency increases more slowly and does not reach as high

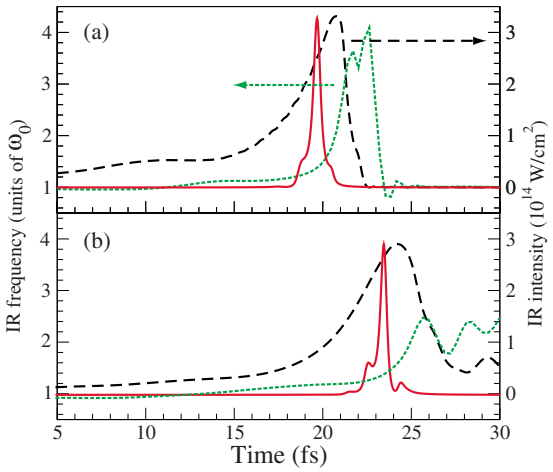

FIG. 5. (Color online) Time dependence of the on-axis intensity and frequency (dashed and dotted lines, respectively) of the self-compressed filament obtained in neon at pressures of 1.0 atm (a) and 0.4 atm (b), respectively, using KPPT ionization rates. The radially integrated time profile of a range of the xuv radiation generated by sending the self-compressed filament into a short, low-pressure argon gas cell is shown with the solid line (in arbitrary units).

a value, which is reasonable given the proportionality of n_2 with the atomic density [see Eq. (7)]. As we discuss in more detail below, the rapid blueshift accompanying the few-cycle pulse formation by filamentation has important consequences for the high-order harmonics generation process as well as on single attosecond pulse formation.

IV. HIGH-ORDER HARMONICS AND ATTOSECOND PULSE GENERATION

We next use the self-compressed pulses generated via filamentation in neon to drive high-order harmonic generation in a separate argon gas cell. The argon medium is short (1 mm) and the pressure is low (0.2 atm). In Fig. 6 we show the radially integrated harmonic spectra at the end of the argon cell, generated by the few-cycle pulses self-compressed at two different neon pressures (as shown in Fig. 5). The two spectra are similar in their cutoff energies and behavior. The main difference between them is the yield: The self-compressed pulse from the low-pressure calculation gives rise to a yield approximately 5 times larger than that from the high-pressure calculations. This can be understood by considering the radial or temporal behavior of the two pulses as shown in Fig. 4. In the low-pressure case more of the energy is temporally confined to the few-cycle pulse and so contributes efficiently to the harmonic generation, whereas in the high-pressure case the off-axis radiation occurs at a slightly different time than the on-axis radiation which is less effective.

A. Effect of the blueshift on high-order harmonic generation

The influence of the rapid frequency blueshift on the generation of attosecond pulses can be understood from a dis-

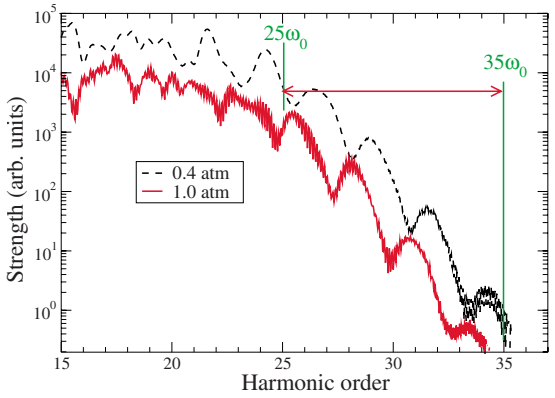

FIG. 6. (Color online) Harmonic spectra generated in a low-pressure argon gas by the self-compressed pulses formed by filamentation in neon, at neon pressures of 1 atm (solid line) and 0.4 atm (dashed line). The spectral ranges used to calculate the xuv time profiles shown in Fig. 5 are indicated.

cussion of the so-called cutoff law for high-order harmonic generation, which relates the highest frequencies that can be generated to the intensity and frequency of the driving field [37],

$$\hbar\omega_{\text{cutoff}} = U_i + 3.2U_p, \tag{8}$$

where U_i denotes the ionization potential of the gas and the ponderomotive energy

$$U_p \equiv \frac{e^2 I}{2\epsilon_0 c m_e \omega^2} \tag{9}$$

is the mean kinetic energy of the free electrons oscillating in the laser field at frequency ω. From Eqs. (8) and (9), it can be readily seen that a Fourier transform limited pulse at frequency ω_0 would give a higher cutoff energy than that of a blueshifted pulse having the same peak intensity but a larger frequency $\omega > \omega_0$ around the peak of the pulse.

Both driving pulses have similar on-axis peak intensities, as shown in Fig. 5, around 3×10^{14} W/cm^2, which does not depend on pressure [35,36]. At this intensity, the cutoff law (8) applied to a Fourier transform limited pulse at frequency ω_0 corresponding to 800 nm would predict a single-atom cutoff energy of approximately $45\omega_0$, significantly above the cutoff energy of the spectra in Fig. 6. Even including estimated effects of radial and temporal averaging in the macroscopic medium, which has been empirically shown to reduce the coefficient in front of U_p to between 2 and 2.5 [39], one would expect a cutoff energy of approximately $35\omega_0$. In Ref. [12] we showed that the reduced cutoff energy is due to the rapid blueshift. We calculated the "instantaneous cutoff frequency" that could be expected from the driving pulse in Fig. 5(a), by inserting the time-dependent intensity and frequency into Eq. (8). The instantaneous cutoff reaches its highest value of $28\omega_0$ at time $t=19.5$ fs, about 1.5 fs before the peak of the intensity in Fig. 5(a). The value of the maximum instantaneous cutoff energy is in much better agreement with the results in Fig. 6.

We calculate the time structure of the generated xuv radiation by spectrally selecting a $10\omega_0$ wide range of frequen-

cies close to the cutoff energy, and inverse Fourier transforming to the time domain. If the driving pulse had been transform-limited with a FWHM duration of 4–5 fs, and a carrier-envelope phase of zero (corresponding to a cosinelike carrier), one would expect that spectral selection of the end of the plateau and beginning of the cutoff region would lead to an isolated attosecond pulse as demonstrated in [40].

However, in our case the driving pulse is not transform limited but rather experiences a large blueshift of the instantaneous frequency. This has two consequences: (i) The highest energies beyond the cutoff energies are generated not at the time where the intensity peaks, but about 1.5 fs earlier as discussed above, (ii) the harmonics at the end of the plateau region (radiation between approximately 20 and $24\omega_0$) are generated both during the rising edge of the pulse and at the peak of the pulse and will therefore always give rise to two attosecond bursts in the xuv time profile. In order to generate an isolated attosecond xuv pulse, we are forced to select harmonics from a range beyond the cutoff energy which limits the energy content of the xuv pulse. The xuv pulses resulting from selecting the spectral range between $25\omega_0$ and $35\omega_0$ are shown by the solid lines in Figs. 5(a) and 5(b), for the two different neon filamentation pressures. The durations of the two pulses are 560 as (a) and 430 as (b). Note that both pulses are emitted substantially before the peaks of the driving pulse intensities as a consequence of a combined time—frequency gating: The increasing intensity of the driving pulse shapes the rising edge of the xuv pulse and the blueshift at the peak and in the trailing part of the driving pulse turns off the emission of the highest xuv energies [12].

We note that our use of the strong field approximation, which is not in general expected to be accurate at large driving frequencies, is justified by the fact that we are using the highest xuv frequencies to synthesize the isolated attosecond pulses, which are emitted while the instantaneous frequency is still only 1.2–1.3 times its original value. In addition, Krause, Schafer, and Kulander did extensive numerical calculations of harmonic spectra for different atoms, generated by driving fields of different wavelengths and intensities [37,38]. They showed that the cutoff law predicts the cutoff energy remarkably well even for very small ponderomotive energies, even substantially smaller than the ionization potential. Lewenstein *et al.* [27], also investigated the regime of small ponderomotive energies and found the corrections to the cutoff law to be very slowly varying with the ponderomotive energy. We therefore expect that isolated attosecond pulses can be similarly synthesized from the highest frequencies of the spectrum obtained from a more accurate calculation of the harmonic generation, in spite of the rapidly changing cutoff energy.

B. Effect of the carrier envelope phase

The filamentation calculations are based on an envelope model which does not give any information on the carrier envelope phase (CEP). From experiments, it is known that the filamentation process preserves the CEP lock during self-compression [6,41]. For HHG with the self-compressed pulse, the CEP is an important parameter since the peak of the electric field can vary substantially as it is shifted under the envelope with the CE phase. Figure 7 shows the effect of arbitrarily changing the driving pulse CEP on the spectral and temporal profiles of the harmonics in the cutoff region.

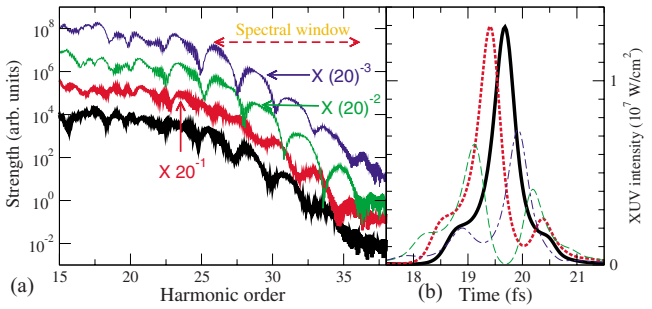

FIG. 7. (Color online) xuv spectra (a) and time profiles (b) calculated with different carrier envelope phases of the driving field corresponding to the self-compressed filament obtained in 1 atm of neon. The different spectra have been separated by a scaling factor for clarity, and corresponds to CEPs of 0, $\pi/4$, $\pi/2$, and $3\pi/4$ starting from below. The corresponding time profiles using the spectral range from $26\omega_0$ to $36\omega_0$ are shown with solid, dotted, dashed, and dotted-dashed lines, respectively.

The overall structure of the spectrum does not change with CEP, but the position of the frequency modulations near the cutoff changes significantly. This happens because the harmonic radiation is generated with an intrinsic phase which is proportional to the instantaneous intensity of the driving field, and therefore depends on time. This means that each harmonic is strongly chirped and neighboring harmonics overlap substantially. As the CEP is changed and the peaks of the electric field are shifted under the intensity envelope, the bursts of harmonic radiation are also shifted in time which means that a different part of the harmonic frequency range will be sampled. This is similar to the CEP-dependent shift of the cutoff harmonics observed by Baltuska and co-workers [42]. Furthermore, the relative strength of the harmonic bursts will vary because of the short duration of the driving pulse. This leads to a shift of each harmonic frequency and more generally to a shift of the entire modulation pattern. The variation of the xuv time structure with CEP is shown in Fig. 7(b). As is indicated on the spectra in (a), we are showing the radially integrated time profile of radiation between $25\omega_0$ and $36\omega_0$. It is quite remarkable that all the spectra are modulated, even though a few of them correspond to a single attosecond pulse. This means that the spectrum cannot be used to diagnose whether a single attosecond pulse has been produced. Instead, one must perform a direct time-domain characterization.

V. CONCLUDING REMARKS

We have investigated the generation of few-cycle pulses via filamentation in noble gases. We showed that the propagation of a 30 fs infrared pulse with a few mJ of energy through each of the noble gases xenon, krypton, argon, and neon at approximately atmospheric pressure leads to the generation of few-cycle pulses with peak intensities of

10^{13}–10^{14} W/cm^2. Although self-compression already starts during the self-focusing stage before the filament is formed, the pulse duration decreases dramatically due to the depletion of the intense part of the pulse which occurs beyond the nonlinear focus. This depletion gives rise to a split pulse. The plasma generated by the leading split pulse makes the process asymmetric and delays the formation of the trailing split pulse. Isolated self-compressed pulses are then obtained at several propagation distances, which depend on the details of the difference in the refocusing dynamics for the leading and trailing pulses. Immediately beyond the nonlinear focus, an isolated few-cycle pulse is usually obtained with a nearly flat temporal phase [7,43], so that it is interesting to extract the pulse at this stage [11]. However, the shortest self-compressed pulses with duration smaller than two cycles at the laser frequency are most often obtained at the end of the filament. The peak intensity in a filament is saturated [14], and the saturation value is large as the ionization rate of the medium is small or the nonlinear index coefficient is large. We found that the most intense self-shortened filaments are obtained for gases with the largest ionization potential, i.e., for neon. In this respect, helium must be even better. We showed that for an input pulse with a given duration and containing a given number of critical powers for self-focusing, an optimal compression ratio exists for a pressure smaller than 1 atm (0.4 atm for $P_{in}/P_{cr}=1.7$ and 30 fs input pulses). Since filaments in low-pressure gases have larger diameters [35], this suggests a possible up-scaling of the energy content of self-compressed filaments in low-pressure gas cells, by decreasing the pressure as the input pulse energy is increased. As an additional advantage, self-compressed filaments generated in low-pressure gas cells could be directly used for HHG in the same cell.

To drive high-order harmonic generation and attosecond pulse formation in noble gases, it is necessary to have intensities above 10^{14} W/cm^2. Our calculations indicate that the filamentation-driven self-compression process that leads to few-cycle pulses with such high peak intensities also leads to a rapid blueshift of the instantaneous laser frequency close to the peak of the pulse. This blueshift was recently interpreted as resulting from the interplay between angular dispersion and optical shocks, and is unavoidable in filamentation [44]. We discussed above that this blueshift is not advantageous for generating isolated attosecond pulses, since it means that only the highest xuv frequencies beyond the cutoff energy are emitted in a single burst.

In an experiment, it may therefore be necessary to compensate for the frequency modulation in between the self-compression stage and the harmonic generation stage. Several experimental groups are already using recompression mirrors after the filamentation stage, in order to control the spectral or temporal phase and to compensate for dispersive effects of propagation through the exit window at the end of the filamentation cell, and through the air between the compression and the target stages [6–8,10,45]. Other groups have reported measurement of longer (3–4 cycles) pulses generated by filamentation, without using chirped mirrors. However, no consensus has been reached regarding the chirp carried by self-shortened filament: Self-compressed pulses with small but negative chirp were measured [46], as well as transform limited pulses having undergone a compensation of the positive chirp induced by their propagation beyond the filament by the negative dispersion in the exit window of the gas cell [41]. These controversial results may be explained by the recent demonstration of the subdispersive and subdiffractive propagation of the wave packet issuing from a filament in a gas [47]. This behavior is due to the spontaneous transformation of the pulse undergoing filamentation into a conical wave packet that inherently carries angular dispersion featured by the medium in which it is generated [9,16,17,48–50]. This conical wave can be viewed as a stationary mode of the linear propagation equation governing the wave packet evolution after the filament. Notably, it is fully space-time coupled and not describable as a conventional optical structure by separation of the time and transverse coordinates. The chirp induced by the propagation of these waves in a different dispersive medium (e.g., the exit windows of the gas cell) cannot simply be assumed to correspond to that experienced by a Gaussian pulse and cannot be compensated by chirped mirrors which act only on the temporal chirp but not on angular dispersion. The development of an optical device allowing proper compensation of the chirp resulting from self-compressed filaments may therefore be necessary for filamentation to become a standard source of intense few-cycle pulses.

ACKNOWLEDGMENTS

This material is based upon work supported by the National Science Foundation through Grant No. PHY-0449235.

[1] M. Hentschel, R. Kienberger, C. Spielmann, G. A. Reider, N. Milosevic, T. Brabec, P. Corkum, U. Heinzmann, M. Drescher, and F. Krausz, Nature (London) **414**, 509 (2001).

[2] P. M. Paul, E. S. Toma, P. Breger, G. Mullot, F. Augé, P. Balcou, H. G. Muller, and P. Agostini, Science **292**, 1689 (2001).

[3] M. Nisoli, S. de Silvestri, O. Svelto, R. Szipöcz, K. Ferencz, C. Spielmann, S. Sartania, and F. Krausz, Opt. Lett. **22**, 522 (1997).

[4] A. Couairon and A. Mysyrowicz, Phys. Rep. **441**, 47 (2007).

[5] S. L. Chin, S. A. Hosseini, W. Liu, Q. Luo, F. Théberge, N. Aközbek, A. Becker, V. Kandidov, O. Kosareva, and H. Schröder, Can. J. Phys. **83**, 863 (2005).

[6] C. P. Hauri, W. Kornelis, F. W. Helbing, A. Heinrich, A. Couairon, A. Mysyrowicz, J. Biegert, and U. Keller, Appl. Phys. B: Lasers Opt. **79**, 673 (2004).

[7] A. Couairon, J. Biegert, C. P. Hauri, W. Kornelis, F. W. Helbing, U. Keller, and A. Mysyrowicz, J. Mod. Opt. **53**, 75 (2006).

[8] A. Guandalini, P. Eckle, M. Anscombe, P. Schlup, J. Biegert,

and U. Keller, J. Phys. B **39**, S257 (2006).
[9] D. Faccio, M. A. Porras, A. Dubietis, G. Tamošauskas, E. Kučinskas, A. Couairon, and P. Di Trapani, Opt. Commun. **265**, 672 (2006).
[10] A. Zaïr, A. Guandalini, F. Schapper, M. Holler, J. Biegert, L. Gallmann, U. Keller, A. Couairon, M. Franco, and A. Mysyrowicz, Opt. Express **15**, 5394 (2007).
[11] A. Couairon, M. Franco, A. Mysyrowicz, J. Biegert, and U. Keller, Opt. Lett. **30**, 2657 (2005).
[12] H. S. Chakraborty, M. B. Gaarde, and A. Couairon, Opt. Lett. **31**, 3662 (2006).
[13] A. Couairon, G. Méchain, S. Tzortzakis, M. Franco, B. Lamouroux, B. Prade, and A. Mysyrowicz, Opt. Commun. **225**, 177 (2003).
[14] A. Couairon, Phys. Rev. A **68**, 015801 (2003).
[15] A. Couairon, L. Sudrie, M. Franco, B. Prade, and A. Mysyrowicz, Phys. Rev. B **71**, 125435 (2005).
[16] D. Faccio, A. Matijosius, A. Dubietis, R. Piskarskas, A. Varanavičius, E. Gaižauskas, A. Piskarskas, A. Couairon, and P. Di Trapani, Phys. Rev. E **72**, 037601 (2005).
[17] A. Couairon, E. Gaižauskas, D. Faccio, A. Dubietis, and P. Di Trapani, Phys. Rev. E **73**, 016608 (2006).
[18] A. Dubietis, A. Couairon, E. Kučinskas, G. Tamošauskas, E. Gaižauskas, D. Faccio, and P. Di Trapani, Appl. Phys. B: Lasers Opt. **84**, 439 (2006).
[19] S. Minardi, A. Gopal, M. Tatarakis, A. Couairon, G. Tamošauskas, R. Piskarskas, A. Dubietis, and P. Di Trapani, Opt. Lett. **33**, 86 (2008).
[20] A. Mysyrowicz, A. Couairon, and U. Keller, New J. Phys. **10**, 025023 (2008).
[21] D. P. Shelton, Phys. Rev. A **42**, 2578 (1990).
[22] A. Dalgarno and A. E. Kingston, Proc. R. Soc. London, Ser. A **259**, 424 (1966).
[23] L. V. Keldysh, Sov. Phys. JETP **20**, 1307 (1965).
[24] A. M. Perelomov, V. S. Popov, and M. V. Terent'ev, Sov. Phys. JETP **23**, 924 (1966).
[25] F. A. Ilkov, J. E. Decker, and S. L. Chin, J. Phys. B **25**, 4005 (1992).
[26] T. Brabec and F. Krausz, Rev. Mod. Phys. **72**, 545 (2000).
[27] M. Lewenstein, P. Balcou, M. Y. Ivanov, A. L'Huillier, and P. B. Corkum, Phys. Rev. A **49**, 2117 (1994).
[28] M. B. Gaarde, K. J. Schafer, A. Heinrich, J. Biegert, and U. Keller, Phys. Rev. A **72**, 013411 (2005).
[29] M. Mlejnek, E. M. Wright, and J. V. Moloney, Phys. Rev. E **58**, 4903 (1998).
[30] A. Sergeev, E. Vanin, L. Stenflo, D. Anderson, M. Lisak, and M. L. Quiroga-Teixeiro, Phys. Rev. A **46**, 7830 (1992).
[31] M. Mlejnek, E. M. Wright, and J. V. Moloney, Opt. Lett. **23**, 382 (1998).
[32] M. Mlejnek, M. Kolesik, J. V. Moloney, and E. M. Wright, Phys. Rev. Lett. **83**, 2938 (1999).
[33] A. Couairon, Eur. Phys. J. D **27**, 159 (2003).
[34] O. G. Kosareva, I. N. Mutarzin, N. A. Panov, A. B. Savel'ev, V. P. Kandidov, and S. L. Chin, Laser Phys. Lett. **4**, 126 (2007).
[35] A. Couairon, M. Franco, G. Méchain, T. Olivier, B. Prade, and A. Mysyrowicz, Opt. Commun. **259**, 265 (2006).
[36] G. Méchain, T. Olivier, M. Franco, A. Couairon, B. Prade, and A. Mysyrowicz, Opt. Commun. **261**, 322 (2006).
[37] J. L. Krause, K. J. Schafer, and K. C. Kulander, Phys. Rev. Lett. **68**, 3535 (1992).
[38] J. L. Krause, K. J. Schafer, and K. C. Kulander, Phys. Rev. A **45**, 4998 (1992).
[39] A. L'Huillier, M. Lewenstein, P. Salières, P. Balcou, M. Y. Ivanov, J. Larsson, and C. G. Wahlström, Phys. Rev. A **48**, R3433 (1993).
[40] R. Kienberger *et al.*, Nature (London) **427**, 817 (2004).
[41] C. P. Hauri *et al.*, Opt. Lett. **32**, 868 (2007).
[42] A. Baltuska *et al.*, Nature (London) **421**, 611 (2003).
[43] O. G. Kosareva, N. A. Panov, D. S. Uryupina, M. V. Kurilova, A. V. Mazhorova, A. B. Savel'ev, R. V. Volkov, V. P. Kandidov, and S. L. Chin, Appl. Phys. B: Lasers Opt. **91**, 35 (2008).
[44] F. Bragheri, D. Faccio, A. Couairon, A. Matijosius, G. Tamošauskas, A. Varanavičius, V. Degiorgio, A. Piskarskas, and P. Di Trapani, Phys. Rev. A **76**, 025801 (2007).
[45] X. Chen, X. Li, J. Liu, P. Wei, X. Ge, R. Li, and Z. Xu, Opt. Lett. **32**, 2402 (2007).
[46] G. Stibenz, N. Zhavoronkov, and G. Steinmeyer, Opt. Lett. **31**, 274 (2006).
[47] D. Faccio, A. Averchi, A. Lotti, P. D. Trapani, A. Couairon, D. Papazoglou, and S. Tzortzakis, Opt. Express **16**, 1565 (2008).
[48] M. Kolesik, E. M. Wright, and J. V. Moloney, Phys. Rev. Lett. **92**, 253901 (2004).
[49] M. A. Porras, A. Dubietis, E. Kučinskas, F. Bragheri, V. Degiorgio, A. Couairon, D. Faccio, and P. Di Trapani, Opt. Lett. **30**, 3398 (2005).
[50] D. Faccio, A. Averchi, A. Couairon, A. Dubietis, R. Piskarskas, A. Matijosius, F. Bragheri, M. A. Porras, A. Piskarskas, and P. Di Trapani, Phys. Rev. E **74**, 047603 (2006).